Published in final edited form as:
Nat Cell Biol. 2008 July ; 10(7): 825–836. doi:10.1038/ncb1744.

Opposing roles for p16^{Ink4a} and p19^{Arf} in senescence and ageing caused by BubR1 insufficiency

Darren J. Baker[1], **Carmen Perez-Terzic**[2], **Fang Jin**[1], **Kevin Pitel**[1], **Nicolas J. Niederländer**[3], **Karthik Jeganathan**[1], **Satsuki Yamada**[3], **Santiago Reyes**[3], **Lois Rowe**[3], **H. Jay Hiddinga**[4], **Norman L. Eberhardt**[4], **Andre Terzic**[3], and **Jan M. van Deursen**[1,4,5]

1 *Department of Pediatric and Adolescent Medicine, Mayo Clinic College of Medicine, Rochester, MN 55905, USA*

2 *Department of Physical Medicine and Rehabilitation, Mayo Clinic College of Medicine, Rochester, MN 55905, USA*

3 *Department of Medicine, Mayo Clinic College of Medicine, Rochester, MN 55905, USA*

4 *Department of Biochemistry and Molecular Biology, Mayo Clinic College of Medicine, Rochester, MN 55905, USA*

Abstract

Expression of *p16^{Ink4a}* and *p19^{Arf}* increases with age in both rodent and human tissues. However, whether these tumour suppressors are effectors of ageing remains unclear, mainly because knockout mice lacking *p16^{Ink4a}* or *p19^{Arf}* die early of tumours. Here, we show that skeletal muscle and fat, two tissues that develop early ageing-associated phenotypes in response to BubR1 insufficiency, have high levels of p16^{Ink4a} and p19^{Arf}. Inactivation of *p16^{Ink4a}* in BubR1-insufficient mice attenuates both cellular senescence and premature ageing in these tissues. Conversely, *p19^{Arf}* inactivation exacerbates senescence and ageing in BubR1 mutant mice. Thus, we identify BubR1 insufficiency as a trigger for activation of the *Cdkn2a* locus in certain mouse tissues, and demonstrate that p16^{Ink4a} is an effector and p19^{Arf} an attenuator of senescence and ageing in these tissues.

Cellular senescence is a state of irreversible growth arrest that can be induced by various cellular stressors[1,2]. The *Cdkn2a* locus encodes two separate tumour suppressors, p16^{Ink4a} (**A001711**), a cyclin-dependent kinase (Cdk) inhibitor that can block G_1–S progression when present above a certain level, and p19^{Arf} (**A001713**), a positive regulator of the transcription factor p53 that integrates and responds to a wide variety of cellular stresses[1,3–5]. Both p16^{Ink4a} and p19^{Arf} are effectors of senescence in cultured cells[6] and their levels increase with ageing in many tissues[7,8]. This has led to speculation that their induction is causally implicated in *in vivo* senescence and organismal ageing. However, rigorous testing of this notion has been difficult because mice that lack *p16^{Ink4a}* or *p19^{Arf}* die of cancer long before they reach the age

5Correspondence should be addressed to J.M.v.D. (e-mail: vandeursen.jan@mayo.edu).

Accession codes. USCD-Nature Signaling Gateway (http://www.signaling-gateway.org): **A001711**, **A001713** and **A003172**

Note: Supplementary Information is available on the Nature Cell Biology website.

AUTHOR CONTRIBUTIONS

D.J.B., C.P.T., F.J., K.P., N.J.N., K.J., S.Y., S.R., L.R., H.J.H. and N.L.E. conducted experiments, prepared the figures and analysed the data; D.J.B., A.T. and J.M.v.D. planned the project and wrote the manuscript; J.M.v.D. supervised the project.

COMPETING FINANCIAL INTERESTS

The authors declare no competing financial interests.

at which normal mice start to develop age-related disorders[1,2]. Recent evidence in middle-aged *p16*^{Ink4a} knockout mice indicates that the age-induced expression of *p16*^{Ink4a} limits the proliferative and regenerative capacity of progenitor populations[9–11]. Yet, whether the increased stem-cell proliferation and tissue regeneration seen in *p16*^{Ink4a} knockouts actually delay onset of age-related pathologies remains unknown because of the limited animal lifespan[1,12].

One approach to study the role of *p16*^{Ink4a} and *p19*^{Arf} in ageing would be to determine whether their respective inactivation by single gene mutations, in mouse models that develop ageing-associated pathologies at an early age, would prevent or delay premature ageing. Mutant mice with low levels of the mitotic checkpoint protein BubR1 (called BubR1 hypomorphic or *BubR1*$^{H/H}$ mice, **A003172**) undergo premature separation of sister chromosomes and develop progressive aneuploidy along with various progeroid phenotypes that include short lifespan, cachectic dwarfism, lordokyphosis (abnormal curvature of the spine), sarcopaenia (age-related skeletal muscle atrophy), cataracts, craniofacial dysmorphisms, arterial stiffening, loss of (subcutaneous) fat, reduced stress tolerance and impaired wound healing[13–15]. During the course of natural ageing, several mouse tissues show a marked decline in BubR1 protein expression, which, combined with the observation that *BubR1*$^{H/H}$ mice age prematurely, suggests a possible role for BubR1 in regulating natural ageing[13–15]. Here we show that certain mouse tissues induce *p16*^{Ink4a} and *p19*^{Arf} in response to BubR1 hypomorphism. Using *BubR1*$^{H/H}$ mice in which these tumour suppressors are lacking, we have demonstrated that p16^{Ink4a} is an effector of cellular senescence and ageing, whereas, p19^{Arf} acts to suppress cellular senescence and ageing.

RESULTS

p16^{Ink4a} inactivation increases the lifespan of *BubR1*$^{H/H}$ mice

To determine the requirement for p16^{Ink4a} in the development of progeroid phenotypes in BubR1-insufficient mice, we bred *BubR1*$^{H/H}$ mice on a *p16*^{Ink4a} homozygous-null genetic background. In total, 86 *BubR1*$^{H/H}$;*p16*$^{Ink4a-/-}$, 192 *BubR1*$^{H/H}$, 160 *BubR1*$^{+/+}$ and 44 *p16*$^{Ink4a-/-}$ mice were generated and monitored for development of age-related phenotypes for a period of one year. Inactivation of *p16*^{Ink4a} extended the lifespan of *BubR1*$^{H/H}$ mice by 25% (Fig. 1a). Although the median lifespan of *BubR1*$^{H/H}$ mice was extended in the absence of p16^{Ink4a}, the maximum lifespan was not, suggesting that the condition(s) that cause(s) death was not rescued by *p16*^{Ink4a} inactivation.

p16^{Ink4a} loss blunts sarcopaenia induced by BubR1 insufficiency

A prominent ageing-associated phenotype of *BubR1*$^{H/H}$ mice is the development of lordokyphosis[13]. The incidence of this phenotype was markedly reduced in *BubR1*$^{H/H}$;*p16*$^{Ink4a-/-}$ animals when compared with *BubR1*$^{H/H}$ mice (Fig. 1b, c). Furthermore, the median time to onset of lordokyphosis was three times longer in *BubR1*$^{H/H}$;*p16*$^{Ink4a-/-}$ mice than in *BubR1*$^{H/H}$ mice (Fig. 1b). Lordokyphosis is associated with both osteoporosis and age-related degenerative loss of muscle mass and strength (sarcopaenia) in wild-type mice of extremely advanced age[16]. Histological evaluation of longitudinal femur sections from kyphotic *BubR1*$^{H/H}$ mice revealed no evidence for osteoporosis (Supplementary Information, Fig. S1a, b). Histopathology on gastrocnemius and paraspinal muscles of 5-month-old *BubR1*$^{H/H}$ mice, however, revealed clear signs of skeletal muscle atrophy and degeneration (Fig. 1d and data not shown). Muscle degeneration was greatly reduced in *BubR1*$^{H/H}$ muscles lacking p16^{Ink4a} (Fig. 1d, e). In addition, abdominal muscles of *BubR1*$^{H/H}$ mice were poorly developed, as revealed by macroscopic analysis and magnetic resonance imaging (Fig. 1f; Supplementary Information, Fig. S1c). Depletion of p16^{Ink4a} resulted in substantial correction

of this defect. These data demonstrate that p16^{Ink4a} has a major role in establishing sarcopaenia in *BubR1*$^{H/H}$ mice.

p16^{Ink4a} limits the regenerative capacity of β cells and has been linked to pancreatic islet atrophy and development of diabetes[9,17,18], which in turn can cause muscle atrophy through accelerated degradation of muscle protein[19]. This prompted us to test whether the sarcopaenia observed in *BubR1*$^{H/H}$ mice might be due to β cell failure. *BubR1*$^{H/H}$ mice showed highly efficient glucose clearance in a glucose-tolerance test (Supplementary Information, Fig. S2a). Complementary blood insulin measurements indicated that insulin sensitivity was not impaired in *BubR1*$^{H/H}$ mice and showed no evidence for insulin resistance (Supplementary Information, Fig. S2b). Furthermore, overall pancreatic morphology, as well as islet size, shape and abundance were similar in 12-month-old *BubR1*$^{H/H}$ and control mice, as verified by histology (Supplementary Information, Fig. S2c). Consistently, *p16^{Ink4a}* expression in the pancreas was not significantly elevated in *BubR1*$^{H/H}$ mice, compared with *BubR1*$^{+/+}$ counterparts. Thus, sarcopaenia in *BubR1*$^{H/H}$ mice is unlikely to be caused by p16^{Ink4a}-mediated β cell degeneration or insulin resistance.

BubR1 and p16^{Ink4a} levels are inversely linked in skeletal muscle

To determine whether BubR1 may have a role in normal skeletal muscle ageing, we measured BubR1 protein levels in skeletal muscle of young and old wild-type mice by western blot analysis. Gastrocnemius muscles had considerably higher levels of BubR1 protein at 2 months than at 35 months of age (Fig. 2a; Supplementary Information, Fig. S6a). *BubR1* transcripts were undetectable by qRT–PCR in the gastrocnemius of 35-month-old mice but were readily present at 2 months (data not shown), suggesting that reduced *BubR1* transcriptional activity contributes to the decline in BubR1 protein levels at advanced age. In contrast to *BubR1* transcription, *p16^{Ink4a}* transcription increased markedly with age in gastrocnemius muscles of old wild-type mice (Fig. 2b). Gastrocnemius of 2- and 5-month-old *BubR1*$^{H/H}$ mice also had high *p16^{Ink4a}* transcript levels (Fig. 2b), providing evidence for an inverse relationship between *BubR1* and *p16^{Ink4a}* expression. To characterize this relationship further, we measured *p16^{Ink4a}* expression in gastrocnemius of 3-week-old *BubR1*$^{H/H}$ mice, when skeletal muscle atrophy is histologically undetectable (Supplementary Information, Fig. S2d). Transcript levels of *p16^{Ink4a}* were similarly elevated for 3-week-old, and 2- and 5-month-old mice (Fig. 2b), indicating that *p16^{Ink4a}* induction is an early response to BubR1 hypomorphism that precedes histological signs of sarcopaenia.

Increased expression of *p16^{Ink4a}* with age in adult stem cells is associated with reduced tissue repair and regeneration in several mouse tissues[9–12]. To explore whether p16^{Ink4a}-mediated exhaustion of myogenic stem-cell potential might contribute to premature sarcopaenia in *BubR1*$^{H/H}$ mice, *in vitro* myoblast-to-myofibre differentiation assays were performed on gastrocnemius muscles from 5-month-old wild-type, *BubR1*$^{H/H}$ and *BubR1*$^{H/H}$;*p16$^{Ink4a-/-}$* mice. In these assays, the average number of myotubes obtained per milligram of muscle tissue was about 7-fold lower in *BubR1*$^{H/H}$ mice than in wild-type mice (Fig. 2c). By contrast, only a 2-fold reduction in myotube formation was observed in *BubR1*$^{H/H}$ mice lacking p16^{Ink4a}. To confirm these data, 5-month-old wild-type, *BubR1*$^{H/H}$ and *BubR1*$^{H/H}$;*p16$^{Ink4a-/-}$* mice were challenged to regenerate muscle fibres by injection of cardiotoxin, a 60-amino-acid polypeptide that causes acute injury by rapidly destroying muscle fibres[20]. Consistent with our *in vitro* data, muscle regeneration was overtly delayed in *BubR1*$^{H/H}$ mice, but not in *BubR1*$^{H/H}$;*p16$^{Ink4a-/-}$* counterparts (Fig. 2d). Collectively, these data indicate that p16^{Ink4a} promotes sarcopaenia in *BubR1*$^{H/H}$ mice, at least in part, by impairing muscle regeneration.

p16^{Ink4a} loss attenuates ageing in selective BubR1 hypomorphic tissues

Loss of p16^{Ink4a} caused a modest, yet significant, delay in the latency of cataract formation in *BubR1*$^{H/H}$ mice (Fig. 3a). Aged skin is characterized by reduced dermal thickness and subcutaneous adipose tissue, both of which are observed in *BubR1*$^{H/H}$ mice at young ages[13]. At 2 months of age, *BubR1*$^{H/H}$, *BubR1*$^{H/H}$;*p16*$^{Ink4a-/-}$ and *p16*$^{Ink4a-/-}$ mice had similar amounts of subdermal adipose tissue (Fig. 3b). As expected, the mean thickness of the subcutaneous adipose layer decreased notably in 5-month-old *BubR1*$^{H/H}$ mice. This decline was not accompanied by increased fat storage in liver tissue (Supplementary Information, Fig. S2e). The decrease in subcutaneous fat was much less severe in age-matched *BubR1*$^{H/H}$;*p16*$^{Ink4a-/-}$ mice (Fig. 3b), indicating that p16^{Ink4a} is, at least in part, responsible for loss of subcutaneous adipose tissue in *BubR1*$^{H/H}$ mice. Tolerance of anaesthetic stress was also greatly improved in *BubR1*$^{H/H}$;*p16*$^{Ink4a-/-}$ mice (Supplementary Information, Table S1), as was adipose tissue deposition (Supplementary Information, Fig. S2f). However, several progeroid symptoms seen in *BubR1*$^{H/H}$ mice remained unchanged following loss of p16^{Ink4a}, including dwarfism, dermal thinning, arterial wall stiffening and infertility (Supplementary Information, Table S1 and data not shown). No progeroid phenotypes of *BubR1*$^{H/H}$ mice were aggravated by p16^{Ink4a} loss.

The differential corrective effects of *p16*^{Ink4a} disruption on individual progeroid phenotypes suggest tissue-specific differences in engagement of the p16^{Ink4a} pathway in the cellular response to BubR1 deficiency. *BubR1*$^{H/H}$ tissues in which p16^{Ink4a} loss causes a significant delay of premature ageing, such as eye and (subdermal) adipose tissue, showed strong induction of *p16*^{Ink4a} expression in response to BubR1 hypomorphism (Fig. 3c, d; Supplementary Information, Fig. S6b, c). *BubR1*$^{H/H}$ tissues in which *p16*^{Ink4a} inactivation has no discernible corrective effect, such as dermis, brain, aorta, testis and ovary, did not exhibit significant *p16*^{Ink4a} induction (Fig. 3c and data not shown). Furthermore, mutant tissues that are not subjected to premature ageing, including lung, pancreas, colon and liver[13], maintained low *p16*^{Ink4a} expression levels. Together, these data demonstrate that *p16*^{Ink4a} is activated in a subset of tissues in *BubR1*$^{H/H}$ mice, where it contributes to progeroid phenotypes.

p16^{Ink4a} loss attenuates *in vivo* senescence

BubR1 is a putative E2F-regulated gene[21] and loss of p16^{Ink4a} leads to increased E2F transcriptional activity[22]. Accordingly, attenuation of ageing in skeletal muscle, fat and eye may be the result of increased *BubR1* gene expression. However, this is unlikely as *BubR1* transcript levels in these tissues were not affected by loss of p16^{Ink4a} (Fig. 4a). As p16^{Ink4a} is an effector of cellular senescence, *p16*^{Ink4a} deletion may delay ageing in hypomorphic mice by decreasing senescence. As shown in Fig. 4b, *BubR1*$^{H/H}$ adipose tissue expresses high levels of senescence-associated (SA)-β-galactosidase, a marker of cellular senescence[23]. SA-β-galactosidase staining was much lower in adipose tissue of *BubR1*$^{H/H}$;*p16*$^{Ink4a-/-}$ mice (Fig. 4b). Skeletal muscles of 2-month-old *BubR1*$^{H/H}$ mice did not stain positive for SA-β-galactosidase but expressed high levels of several other senescence-associated genes, including *Igfbp2*, *Nrg1*, *Mmp13* and *PAI-1*[24–27] (Fig. 4c). Expression of these markers was decreased markedly in skeletal muscles of age-matched *BubR1*$^{H/H}$;*p16*$^{Ink4a-/-}$ mice. A key feature of senescence is loss of proliferative potential. *In vivo* 5-bromo-2-de-oxyuridine (BrdU) labelling showed that 2-month-old *BubR1*$^{H/H}$ mice had much lower percentages of ycling cells in skeletal muscle and fat than wild-type mice (Fig. 4d). These reductions were less profound in *BubR1*$^{H/H}$;*p16*$^{Ink4a-/-}$ mice. Collectively, these data suggest that BubR1 hypomorphism causes cellular senescence in adipose tissue and skeletal muscle through a p16^{Ink4a}-dependent mechanism. As *p16*^{Ink4a} inactivation attenuates both senescence and ageing in these tissues, the mechanism by which BubR1 hypomorphism accelerates the ageing phenotypes may involve p16^{Ink4a}-induced senescence.

p19^{Arf} is elevated in *BubR1*$^{H/H}$ tissues with high levels of p16^{Ink4a}

Besides *p16*^{Ink4a}, *p19*^{Arf} is expressed at increased levels in many tissues of wild-type mice with advanced age[7], including skeletal muscle (Fig. 5a). Although p19^{Arf} is an established effector of senescence in cultured mouse embryonic fibroblasts (MEFs), its role in senescence and ageing in the context of the whole organism has not been clarified[1,2]. To explore the role of p19^{Arf} in BubR1-mediated ageing, we analysed its relative expression in tissues from 2-month-old *BubR1*$^{H/H}$ and *BubR1*$^{+/+}$ mice. Increased *p19*^{Arf} expression was consistently observed in *BubR1*$^{H/H}$ tissues that were subjected to premature ageing and had high p16^{Ink4a} levels, including skeletal muscle, (subdermal) adipose tissue and eye, but not in tissues that developed age-related pathology in a p16^{Ink4a}-independent fashion or had no age-related phenotypes (Fig. 5b, c; Supplementary Information, Fig. S6b, c and data not shown). Skeletal muscle, (subdermal) adipose tissue and eye from *BubR1*$^{H/H}$ mice lacking p16^{Ink4a} had normal *p19*^{Arf} transcript levels (Fig. 5d), suggesting that the observed increase in *p19*^{Arf} expression is dependent on high p16^{Ink4a} levels. *p15*^{Ink4b}, which encodes a Cdk inhibitor that has been linked to ageing in some tissues[7], was neither increased in *BubR1*$^{H/H}$ tissues with increased *p16*^{Ink4a} and *p19*^{Arf} expression, nor in any other tissue of *BubR1*$^{H/H}$ mice (Supplementary Information, Figs S3a, S6b, c). In contrast to *p16*^{Ink4a} and *p19*^{Arf}, *p15*^{Ink4b} was not expressed at increased levels in skeletal muscles of aged wild-type mice (Supplementary Information, Fig. S3b).

p19^{Arf} disruption accelerates ageing in *BubR1*$^{H/H}$ mice

To determine whether p19^{Arf} also acts as an effector of ageing in *BubR1*$^{H/H}$ mice, 41 *BubR1*$^{H/H}$;*p19*$^{Arf-/-}$ mice were generated and monitored for development of age-related phenotypes. Surprisingly, lordokyphosis developed at a significantly faster rate in *BubR1*$^{H/H}$;*p19*$^{Arf-/-}$ mice than in *BubR1*$^{H/H}$ mice (Fig. 6a, b). Six-week-old *BubR1*$^{H/H}$;*p19*$^{Arf-/-}$ mice had significantly smaller fibres in gastrocnemius and abdominal muscles than age-matched *BubR1*$^{H/H}$ mice (Fig. 6c; Supplementary Information, Fig. S4a), indicating that muscle wasting was accelerated in the absence of p19^{Arf}. Cataract formation was also significantly accelerated when p19^{Arf} was absent (Fig. 6d). Skinned 6-week-old *BubR1*$^{H/H}$;*p19*$^{Arf-/-}$ mice showed overt reductions in deposition of adipose tissue (Fig. 6b). This was confirmed by weighing inguinal adipose tissue (IAT, Fig. 6e). Furthermore, the mean thickness of the subcutaneous adipose layer was significantly smaller in *BubR1*$^{H/H}$;*p19*$^{Arf-/-}$ mice than in *BubR1*$^{H/H}$ mice (0.07 versus 0.11 mm; $P < 0.0001$, two-tailed Mann-Whitney test). Other progeroid features of *BubR1*$^{H/H}$ mice seemed to be unchanged by *p19*^{Arf} inactivation (Supplementary Information, Fig. S4b and Table S1). Taken together, these data indicate that p19^{Arf} acts to delay ageing in response to BubR1 hypomorphism.

One possible explanation for the pro-ageing effect of *p19*^{Arf} inactivation in *BubR1*$^{H/H}$ mice may involve increased expression of p16^{Ink4a}. Consistent with this idea, p16^{Ink4a} levels in skeletal muscle, fat and eye increased markedly when *p19*^{Arf} was knocked out in *BubR1*$^{H/H}$ mice (Fig. 6f, g; Supplementary Information, Fig. S6d). A potential explanation for these results may be that genetic manipulation of *p19*^{Arf} sequences changes the normal regulatory balance in the *Cdkn2* locus, thereby increasing *p16*^{Ink4a} expression. However, disruption of *p19*^{Arf} had no appreciable effect on p16^{Ink4a} levels in tissues undergoing p16^{Ink4a}-independent ageing or lacking age-related pathologies (Fig. 6g), arguing against this possibility.

Inactivation of *p19*^{Arf} increases cellular senescence

Next, we investigated whether p19^{Arf} loss accelerates ageing in *BubR1*$^{H/H}$ mice through increased senescence. Indeed adipose tissue of 6-week-old *BubR1*$^{H/H}$;*p19*$^{Arf-/-}$ mice showed much higher SA-β-galactosidase activity than that of corresponding *BubR1*$^{H/H}$ mice (Fig. 7a). Furthermore, two senescence-associated genes, *Igfbp2* and *Nrg1*, which are expressed at increased levels in gastrocnemius muscles of 6-week-old *BubR1*$^{H/H}$ mice, were further

elevated in corresponding muscles of age-matched *BubR1*$^{H/H}$;*p19*$^{Arf-/-}$ mice (Fig. 7b). *In vivo* BrdU incorporation showed that cell proliferation in skeletal muscle and fat was considerably lower in *BubR1*$^{H/H}$;*p19*$^{Arf-/-}$ mice than in *BubR1*$^{H/H}$ mice (Fig. 7c). Collectively, these data indicate that p19^{Arf} induction in *BubR1*$^{H/H}$ mice functions to prevent or delay senescence and provide further evidence for the notion that *in vivo* senescence promotes ageing.

Distinct *in vivo* and *in vitro* effects of *p16*^{Ink4a} and *19*^{Arf} inactivation on senescence

Previously, we have shown that *BubR1*$^{H/H}$ MEFs express high levels of p16^{Ink4a} and p19^{Arf} and age prematurely[13]. To determine the effects p16^{Ink4a} and p19^{Arf} on cellular senescence in these MEFs, we stained *BubR1*$^{H/H}$;*p16*$^{Ink4a-/-}$ and *BubR1*$^{H/H}$;*p19*$^{Arf-/-}$ MEFs for SA-β-galactosidase. Inactivation of *p19*^{Arf} caused a marked decrease in senescence in *BubR1*$^{H/H}$ MEFs, whereas inactivation of *p16*^{Ink4a} had no effect (Supplementary Information, Fig. S5a, b). Consistently, the percentage of cycling cells was greatly increased in *BubR1*$^{H/H}$;*p19*$^{Arf-/-}$ MEFs, but not in *BubR1*$^{H/H}$;*p16*$^{Ink4a-/-}$ MEFs (Supplementary Information, Fig. S5c, d). Furthermore, *BubR1*$^{H/H}$;*p19*$^{Arf-/-}$ MEFs grew considerably faster than *BubR1*$^{H/H}$ MEFs, but *BubR1*$^{H/H}$;*p16*$^{Ink4a-/-}$ MEFs did not (Supplementary Information, Fig. S5e, f). Immunoblotting showed that the p19^{Arf}–53 pathway remained highly active in *BubR1*$^{H/H}$;*p16*$^{Ink4a-/-}$ MEFs, similarly to *BubR1*$^{H/H}$ MEFs, whereas it was inactive in *BubR1*$^{H/H}$;*p19*$^{Arf-/-}$ MEFs (Supplementary Information, Fig. S5h, g). Together, these data demonstrate that the effects of p16^{Ink4a} and p19^{Arf} ablation on *in vivo* senescence in skeletal muscle and fat of *BubR1*$^{H/H}$ mice are not recapitulated by their effects on *in vitro* senescence in *BubR1*$^{H/H}$ MEFs.

p16^{Ink4a} loss synergizes with BubR1 insufficiency in lung tumorigenesis

BubR1$^{H/H}$ mice show progressive and severe aneuploidy but rarely develop tumours[13]. Activation of *p16*^{Ink4a} or *p19*^{Arf} in response to BubR1 hypomorphism may act to suppress tumorigenesis. To test for this possibility, *BubR1*$^{H/H}$ mice lacking p16^{Ink4a} or p19^{Arf} were monitored for tumour formation. Live *BubR1*$^{H/H}$;*p16*$^{Ink4a-/-}$ and *BubR1*$^{H/H}$ mice showed no overt tumours, but biopsy of moribund or dead animals revealed that *BubR1*$^{H/H}$;*p16*$^{Ink4a-/-}$ mice had significantly more tumours than *BubR1*$^{H/H}$ mice (Fig. 8a). Eight out of nine *BubR1*$^{H/H}$;*p16*$^{Ink4a-/-}$ tumours were lung adenocarcinomas, a type of tumour observed in only one *BubR1*$^{H/H}$ mouse and none of the *p16*$^{Ink4a-/-}$ mice (Fig. 8b). Sarcomas, the most prevalent tumour type in *p16*$^{Ink4a-/-}$ mice, were rare in *BubR1*$^{H/H}$;*p16*$^{Ink4a-/-}$ mice and not present in *BubR1*$^{H/H}$ mice. Thus, the effect of BubR1 insufficiency is synergistic with that of p16^{Ink4a} loss during tumorigenesis in lung epithelial cells, but not in other cell types (see Supplementary Discussion). *BubR1*$^{H/H}$;*p19*$^{Arf-/-}$ and *p19*$^{Arf-/-}$ mice, however, had overlapping tumour-free survival curves (Fig. 8c), indicating that BubR1 insufficiency and p19^{Arf} loss do not synergize in tumorigenesis.

DISCUSSION

Here, we report that inactivation of p16*^{Ink4a}* attenuates the development of age-related pathologies in *BubR1*$^{H/H}$ tissues with elevated p16^{Ink4a}. This shows that induction of *p16*^{Ink4a} by cellular stress resulting from BubR1-insufficiency drives the development of ageing-associated phenotypes, and provides direct evidence for a causal involvement of this tumour suppressor in organismal ageing. Importantly, skeletal muscle and fat, two tissues that are subject to p16^{Ink4a}-dependent ageing when BubR1 levels are low, have higher numbers of replicating cells and show decreased expression of senescence-associated proteins in the absence of p16^{Ink4a}. These observations support the notion that p16^{Ink4a} contributes to ageing-associated pathologies through accumulation of senescent cells. This is a significant finding as evidence that cellular senescence promotes ageing has thus far been largely circumstantial[2,6].

BubR1$^{H/H}$ mouse tissues, in which p16^{Ink4a} is elevated, also have increased p19^{Arf}. However, *p19^{Arf}* inactivation accelerates rather than delays ageing in these tissues, indicating that this tumour suppressor provides anti-ageing activity. This seems surprising, considering that p19^{Arf} is an effector of senescence in cultured cells[2,6]. However, the recent observation that transgenic mice carrying an extra copy of both p19^{Arf} and p53 are protected from ageing-associated damage and live longer than normal mice[28], is consistent with our finding that p19^{Arf} has anti-ageing activity in *BubR1*$^{H/H}$ mice. It has been proposed that the p19^{Arf}–p53 pathway in response to low, chronic stress, may primarily induce genes that promote cell survival and repair, thereby extending lifespan[5,28,29]. High, acute types of stress, on the other hand, may accelerate ageing by triggering a more robust p53 response, causing irreversible cell-cycle arrest and/or apoptosis[5,29–31]. Therefore, one possibility is that p19^{Arf} may elicit a p53 transcriptional response that provides protection against cellular stress resulting from BubR1 hypomorphism, thus delaying the onset of cellular senescence. The observation that skeletal muscle and fat from *BubR1*$^{H/H}$ mice lacking p19^{Arf} accumulate more senescent cells is consistent with this idea. Strong additional support for the conclusion that p19^{Arf} has anti-ageing activity is provided by our unpublished observations indicating that *BubR1*$^{H/H}$ mice lacking p53 phenocopy those lacking p19^{Arf}. Two observations reported here suggest that p19^{Arf} may exert its anti-ageing effect, at least in part, through negative regulation of p16^{Ink4a} expression. First, inactivation of *p19^{Arf}* in *BubR1*$^{H/H}$ mice resulted in increased p16^{Ink4a} expression in skeletal muscle, fat and eye, three tissues that have high p19^{Arf} levels and are subjected to accelerated ageing. Second, inactivation of *p16^{Ink4a}* prevented the induction of *p19^{Arf}* in these *BubR1*$^{H/H}$ tissues. How p19^{Arf} attenuates *p16^{Ink4a}* expression remains to be addressed.

Although inactivation of *p16^{Ink4a}* significantly delays the development of certain ageing-associated phenotypes in *BubR1*$^{H/H}$ mice, it does not completely prevent them. Furthermore, other progeroid phenotypes are not affected by loss of p16^{Ink4a}. These findings suggest that BubR1 hypomorphism engages other progeroid effectors in addition to p16^{Ink4a}. The identity of these effectors is currently unclear and remains to be established. Striking similarities exist between the progeroid phenotypes of *BmalI* knockout and *BubR1*$^{H/H}$ mice[32]. The molecular basis of this similarity is unclear, although, based on the known roles of each protein, it is unlikely that BubR1 and BmalI are functionally connected. However, it is possible that downstream pathways that respond to stress resulting from Bmal1 loss and BubR1 hypomorphism are shared.

METHODS

Generation of compound mutant mice

BubR1$^{H/H}$ mice were generated as described previously[13]. *p16^{Ink4a}* and *p19^{Arf}* knockout mice have been generated previously and were acquired from the Mouse Models of Human Cancers Consortium located at the National Cancer Institute, Frederick[33,34]. All mice were on a mixed 129 × C57BL/6 genetic background. They were housed in a pathogen-free barrier environment for the duration of the study. Experimental procedures involving the use of these laboratory mice were reviewed and approved by the Institutional Animal Care and Use Committee of the Mayo Clinic. Prism software (GraphPad Software) was used for generation of all survival curves and for statistical analyses.

Collection and analysis of tumours

Moribund mice were killed and all major organs were screened for overt tumours using a dissection microscope. Tumours that were collected were processed by standard procedures for histopathology. A Fisher's exact test was used to compare tumour incidence proportions

across the genotypes for mice that developed tumours. Board-certified pathologists assisted in the histological evaluation of tumour sections.

Analysis of progeroid phenotypes

Bi-weekly, mice were screened for the development of overt cataracts by examining dilated eyes with a slit-light. Incidence of lordokyphosis was checked bi-weekly. Mice that showed lordokyphosis for three consecutive monitoring periods were determined to have this condition. Various skeletal muscles were collected and processed for histology as described previously[35,36]. Fibre diameter measurements were performed on cross sections of gastrocnemius and abdominal muscles from 6-week-old male mice ($n = 3$ mice per genotype). A total of 50 fibres were measured per muscle using a calibrated computer program (Olympus MicroSuite Five). Dissection, histology and measurements of dermal and adipose layers of dorsal skin were performed as described previously[16]. Values represent an average of four males. Analysis of arterial wall stiffening was performed as described previously[14]. Measurements of body weight and IAT were performed on 6-week-old males ($n = 3$ per genotype). Oral glucose tolerance tests were performed on 5-month-old male mice ($n = 5$ per genotype) as described by the Jackson Laboratory (www.jax.org). Insulin measurements were performed as described previously[37].

Quantitative real-time PCR

Total RNA was extracted from tissues using a Qiagen RNeasy RNA isolation kit according to the manufacturer's protocol. Transcription into cDNA was performed using random hexamers and SuperScript III reverse transcriptase (Invitrogen) according to the manufacturer's instructions. All PCR reactions used SYBR green PCR Master Mix (Applied Biosystems) to a final volume of 12 μl, with each cDNA sample performed in triplicate in the ABI PRISM 7900 Sequence Detection System (Applied Biosystems) according to the protocol of the manufacturer. All experiments were performed on organs/tissues from at least three different animals in each age group and genotype. The expression of genes was normalized to *GAPDH*. Sequences of primers used for qRT–PCR of $p15^{Ink4b}$ (ref. 38), $p16^{Ink4a}$ (ref. 39), $p19^{Arf}$ (ref. 28), *BubR1* (ref. 40), *Mmp-13* (ref. 41), *PAI-1* (ref. 42), *Igfbp-2* (ref. 43), and *GAPDH* (ref. 44) were as published. Additionally, sequences for *Nrg1* were: forward, CATGGTGAACATAGCGAATGGCC; reverse, CCACAATATGCTCACTGGAGATG A. Statistical differences were determined using an unpaired two-tailed *t* test.

Analysis of satellite-cell function

Analysis of *in vivo* satellite-cell function were carried out as described previously[20]. Briefly, mice anaesthetized with avertin (200 mg kg^{-1}, i.p.) were given a single 50-μl injection of cardiotoxin (10 μM; Calbiochem) into the gastrocnemius muscle. After this injection, the skin incision was closed with a nylon suture. Mice were allowed to recover and then were analysed at both 5 and 18 days post-injection by routine histology. Isolation and culture of skeletal muscle satellite cells were performed as described previously[45]. Briefly, hindlimb muscles of 5-month-old mice were removed and trimmed of excess connective tissue and fat. Minced muscles were subjected to several 15-min rounds of digestion at 37 °C in incubation medium (50% DMEM high glucose (GIBCO)/50% F-12K (CellGro)/168 U ml^{-1} collagenase type II (Worthington)/0.04% Trypsin (GIBCO)). Once fully digested, cells were successively filtered through 70- and 40-μm strainers, collected by centrifugation at 300*g* for 5 min and resuspended in propagation medium (DMEM high glucose/15% FCS (GIBCO)/glutamine (CellGro)/ penicillin-streptomycin (CellGro)). After seven days in culture, differentiation medium (propagation medium with 2% FCS) was applied and cells were fixed seven days after transfer to the medium. Myotube formation was quantified using the total number of myotubes for each sample normalized to the muscle mass extracted.

Magnetic resonance imaging

Magnetic resonance images with a 7-tesla scanner (Bruker) were obtained in 2%-isofluorane anaesthetized mice using a spinecho method as described previously[46]. Digital images were analysed with the Metamorph software (Visitron, Universal Imaging). The ratio of muscle area (paraspinal and chest or abdominal wall muscles) to total body cross-section was measured at the distal thorax and mid-abdomen levels.

In vivo BrdU incorporation

At 24 and 6 h before tissue collection, male mice of various genotypes were injected intraperitoneally with 200 μl of BrdU (10 mg ml^{-1}; Sigma) in PBS. Mice were anaesthetized (avertin, 200 mg kg^{-1}, i.p.) and successively perfused (transcardially) with PBS and 10% formalin. Organs were collected and embedded in paraffin. Five-μm sections were prepared and stained for BrdU according to the manufacturer's protocol (BD Pharmingen). The percentage of BrdU-positive cells was determined by counting total and BrdU-positive nuclei in 10 non-overlapping fields at ×40 magnification (n =3 mice per genotype).

Generation and culture of MEFs

MEFs were generated as described previously[47]. BrdU incorporation assays on MEFs were performed according to the manufacturer's protocol (BD Bioscience). Growth curves were generated as described previously[13]. Three independent MEF lines for each genotype were analysed in both experiments.

SA-β-galactosidase staining

Adherent MEFs were stained with a SA-β-galactosidase activity kit according to manufacturer's protocol (Cell Signaling). Nuclei were stained with Hoechst to determine percentages of cells positive for SA-β-galactosidase activity. The percentage of SA-β-galactosidase-positive cells was the total number of cells positive for SA- β-galactosidase activity divided by the total number of cells (n = 3 independent MEF lines for each genotype at each passage). Adipose tissue depositions were stained for SA-β-galactosidase activity, as described previously[13].

Western blot analyses

Western blot analyses were carried out as described previously[48]. Antibodies for senescence-associated proteins were as described[13,16]. The antibody for $p15^{Ink4b}$ was a gift from M. Barbacid[49].

Acknowledgements

We thank Paul Galardy, Rick Bram, Randy Faustino, Amy Tang, Robin Ricke and Jim Kirkland for critical reading of the manuscript or helpful discussions. We would like to thank Mariano Barbacid for the generous gift of anti-$p15^{Ink4b}$ antibody. This work was supported by grants from the National Institutes of Health, the Ted Nash Foundation and the Ellison Medical Foundation to J.v.D.

References

1. Collado M, Blasco MA, Serrano M. Cellular senescence in cancer and aging. Cell 2007;130:223–233. [PubMed: 17662938]
2. Campisi J, d'Adda di Fagagna F. Cellular senescence: when bad things happen to good cells. Nature Rev Mol Cell Biol 2007;8:729–740. [PubMed: 17667954]
3. Sharpless NE, DePinho RA. The INK4A/ARF locus and its two gene products. Curr Opin Genet Dev 1999;9:22–30. [PubMed: 10072356]

4. Sherr CJ, Weber JD. The ARF/p53 pathway. Curr Opin Genet Dev 2000;10:94–99. [PubMed: 10679383]
5. Vousden KH, Lane D. P p53 in health and disease. Nature Rev Mol Cell Biol 2007;8:275–283. [PubMed: 17380161]
6. Kim WY, Sharpless NE. The regulation of INK4/ARF in cancer and aging. Cell 2006;127:265–275. [PubMed: 17055429]
7. Krishnamurthy J, et al. Ink4a/Arf expression is a biomarker of aging. J Clin Invest 2004;114:1299–1307. [PubMed: 15520862]
8. Zindy F, Quelle DE, Roussel MF, Sherr CJ. Expression of the p16INK4a tumor suppressor versus other INK4 family members during mouse development and aging. Oncogene 1997;15:203–211. [PubMed: 9244355]
9. Krishnamurthy J, et al. p16INK4a induces an age-dependent decline in islet regenerative potential. Nature 2006;443:453–457. [PubMed: 16957737]
10. Janzen V, et al. Stem-cell ageing modified by the cyclin-dependent kinase inhibitor p16INK4a. Nature 2006;443:421–426. [PubMed: 16957735]
11. Molofsky AV, et al. Increasing p16INK4a expression decreases forebrain progenitors and neurogenesis during ageing. Nature 2006;443:448–452. [PubMed: 16957738]
12. Beausejour CM, Campisi J. Ageing: balancing regeneration and cancer. Nature 2006;443:404–405. [PubMed: 16957734]
13. Baker DJ, et al. BubR1 insufficiency causes early onset of aging-associated phenotypes and infertility in mice. Nature Genet 2004;36:744–749. [PubMed: 15208629]
14. Matsumoto T, et al. Aging-associated vascular phenotype in mutant mice with low levels of BubR1. Stroke 2007;38:1050–1056. [PubMed: 17272762]
15. Hartman TK, Wengenack TM, Poduslo JF, van Deursen JM. Mutant mice with small amounts of BubR1 display accelerated age-related gliosis. Neurobiol Aging 2007;28:921–927. [PubMed: 16781018]
16. Baker DJ, et al. Early aging-associated phenotypes in Bub3/Rae1 haploinsufficient mice. J Cell Biol 2006;172:529–540. [PubMed: 16476774]
17. Rane SG, et al. Loss of Cdk4 expression causes insulin-deficient diabetes and Cdk4 activation results in β-islet cell hyperplasia. Nature Genet 1999;22:44–52. [PubMed: 10319860]
18. Sharpless NE, DePinho RA. How stem cells age and why this makes us grow old. Nature Rev Mol Cell Biol 2007;8:703–713. [PubMed: 17717515]
19. Price SR, Mitch WE. Mechanisms stimulating protein degradation to cause muscle atrophy. Curr Opin Clin Nutr Metab Care 1998;1:79–83. [PubMed: 10565334]
20. Koh TJ, Bryer SC, Pucci AM, Sisson TH. Mice deficient in plasminogen activator inhibitor-1 have improved skeletal muscle regeneration. Am J Physiol Cell Physiol 2005;289:C217–C223. [PubMed: 15716324]
21. Fridlyand J, et al. Breast tumor copy number aberration phenotypes and genomic instability. BMC Cancer 2006;6:96. [PubMed: 16620391]
22. Hengstschlager M, et al. Loss of the p16/MTS1 tumor suppressor gene causes E2F-mediated deregulation of essential enzymes of the DNA precursor metabolism. DNA Cell Biol 1996;15:41–51. [PubMed: 8561896]
23. Dimri GP, et al. A biomarker that identifies senescent human cells in culture and in aging skin *in vivo*. Proc Natl Acad Sci USA 1995;92:9363–9367. [PubMed: 7568133]
24. West MD, Pereira-Smith OM, Smith JR. Replicative senescence of human skin fibroblasts correlates with a loss of regulation and overexpression of collagenase activity. Exp Cell Res 1989;184:138–147. [PubMed: 2551704]
25. Wang S, Moerman EJ, Jones RA, Thweatt R, Goldstein S. Characterization of IGFBP-3, PAI-1 and SPARC mRNA expression in senescent fibroblasts. Mech Ageing Dev 1996;92:121–132. [PubMed: 9080393]
26. Shelton DN, Chang E, Whittier PS, Choi D, Funk WD. Microarray analysis of replicative senescence. Curr Biol 1999;9:939–945. [PubMed: 10508581]

27. Linskens MH, et al. Cataloging altered gene expression in young and senescent cells using enhanced differential display. Nucleic Acids Res 1995;23:3244–3251. [PubMed: 7667101]
28. Matheu A, et al. Delayed ageing through damage protection by the Arf/p53 pathway. Nature 2007;448:375–379. [PubMed: 17637672]
29. Serrano M, Blasco MA. Cancer and ageing: convergent and divergent mechanisms. Nature Rev Mol Cell Biol 2007;8:715–722. [PubMed: 17717516]
30. Varela I, et al. Accelerated ageing in mice deficient in Zmpste24 protease is linked to p53 signalling activation. Nature 2005;437:564–568. [PubMed: 16079796]
31. Cao L, Li W, Kim S, Brodie SG, Deng CX. Senescence, aging, and malignant transformation mediated by p53 in mice lacking the Brca1 full-length isoform. Genes Dev 2003;17:201–213. [PubMed: 12533509]
32. Kondratov RV, Kondratova AA, Gorbacheva VY, Vykhovanets OV, Antoch MP. Early aging and age-related pathologies in mice deficient in BMAL1, the core componentof the circadian clock. Genes Dev 2006;20:1868–1873. [PubMed: 16847346]
33. Sharpless NE, et al. Loss of p16Ink4a with retention of p19Arf predisposes mice to tumorigenesis. Nature 2001;413:86–91. [PubMed: 11544531]
34. Sharpless NE, Ramsey MR, Balasubramanian P, Castrillon DH, DePinho RA. The differential impact of p16(INK4a) or p19(ARF) deficiency on cell growth and tumorigenesis. Oncogene 2004;23:379–385. [PubMed: 14724566]
35. Engel WK, Cunningham GG. Rapid examination of muscle tissue, an improved trichrome method for fresh-frozen biopsy sections. Neurology 1963;13:919–923. [PubMed: 14079951]
36. Kane GC, et al. ATP-sensitive K^+ channel knockout compromises the metabolic benefit of exercise training, resulting in cardiac deficits. Diabetes 2004;53(suppl 3):S169–S175. [PubMed: 15561907]
37. Baur JA, et al. Resveratrol improves health and survival of mice on a high-calorie diet. Nature 2006;444:337–342. [PubMed: 17086191]
38. Krimpenfort P, et al. p15Ink4b is a critical tumour suppressor in the absence of p16Ink4a. Nature 2007;448:943–946. [PubMed: 17713536]
39. Edwards MG, et al. Gene expression profiling of aging reveals activation of a p53-mediated transcriptional program. BMC Genomics 2007;8:80. [PubMed: 17381838]
40. Yuan B, et al. Increased expression of mitotic checkpoint genes in breast cancer cells with chromosomal instability. Clin Cancer Res 2006;12:405–410. [PubMed: 16428479]
41. Maes C, et al. Soluble VEGF isoforms are essential for establishing epiphyseal vascularization and regulating chondrocyte development and survival. J Clin Invest 2004;113:188–199. [PubMed: 14722611]
42. Asahi M, et al. Protective effects of statins involving both eNOS and tPA in focal cerebral ischemia. J Cereb Blood Flow Metab 2005;25:722–729. [PubMed: 15716855]
43. Ohlson N, Bergh A, Persson ML, Wikstrom P. Castration rapidly decreases local insulin-like growth factor-1 levels and inhibits its effects in the ventral prostate in mice. Prostate 2006;66:1687–1697. [PubMed: 16998818]
44. Jeong YJ, et al. Optimization of real time RT–PCR methods for the analysis of gene expression in mouse eggs and preimplantation embryos. Mol Reprod Dev 2005;71:284–289. [PubMed: 15806558]
45. Beauchamp JR, Morgan JE, Pagel CN, Partridge TA. Dynamics of myoblast transplantation reveal a discrete minority of precursors with stem cell-like properties as the myogenic source. J Cell Biol 1999;144:1113–1122. [PubMed: 10087257]
46. Yamada S, et al. Protection conferred by myocardial ATP-sensitive K^+ channels in pressure overload-induced congestive heart failure revealed in KCNJ11 Kir6.2-null mutant. J Physiol 2006;577:1053–1065. [PubMed: 17038430]
47. Babu JR, et al. Rae1 is an essential mitotic checkpoint regulator that cooperates with Bub3 to prevent chromosome missegregation. J Cell Biol 2003;160:341–353. [PubMed: 12551952]
48. Kasper LH, et al. CREB binding protein interacts with nucleoporin-specific FG repeats that activate transcription and mediate NUP98-HOXA9 oncogenicity. Mol Cell Biol 1999;19:764–776. [PubMed: 9858599]

49. Latres E, et al. Limited overlapping roles of P15(INK4b) and P18(INK4c) cell cycle inhibitors in proliferation and tumorigenesis. EMBO J 2000;19:3496–3506. [PubMed: 10880462]

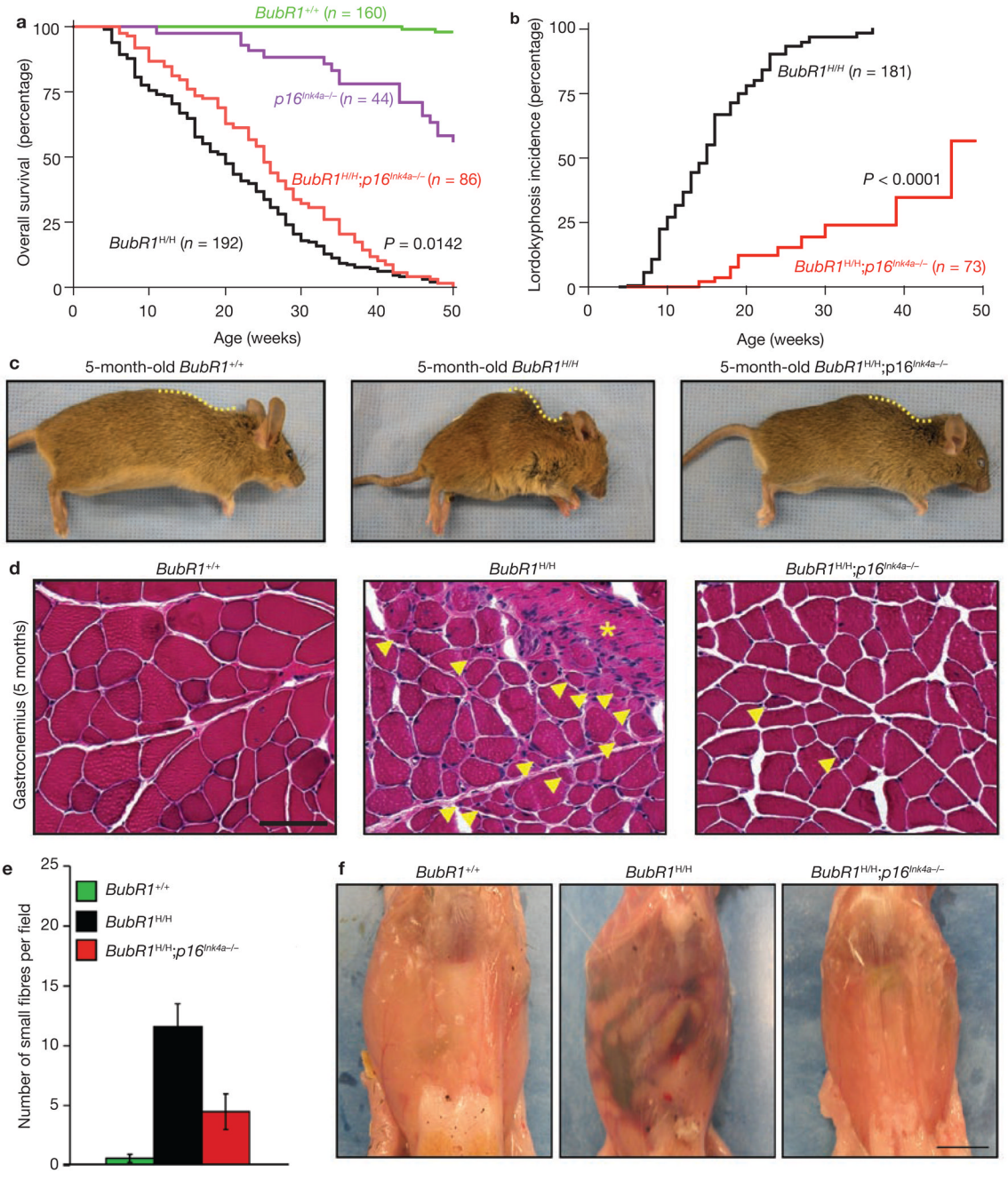

Figure 1.

Ablation of p16^{Ink4a} in *BubR1*$^{H/H}$ mice extends lifespan and attenuates sarcopaenia. (**a**) Overall survival curves for wild-type, *p16*$^{Ink4a-/-}$, *BubR1*$^{H/H}$ and *BubR1*$^{H/H}$;*p16*$^{Ink4a-/-}$ mice. The median overall survival of combined *BubR1*$^{H/H}$;*p16*$^{Ink4a-/-}$ mice is 25 weeks, a 25% extension in lifespan compared with *BubR1*$^{H/H}$ animals. We note that the *p16*$^{Ink4a-/-}$, *BubR1*$^{H/H}$ and *BubR1*$^{H/H}$;*p16*$^{Ink4a-/-}$ curves are all significantly different from the wild-type (*BubR1*$^{+/+}$) curve ($P < 0.0001$, log-rank tests). Moreover, the *BubR1*$^{H/H}$;*p16*$^{Ink4a-/-}$ curve is significantly different from the *BubR1*$^{H/H}$ curve ($P = 0.0142$). (**b**) Incidence and latency of lordokyphosis in *BubR1*$^{H/H}$ and *BubR1*$^{H/H}$;*p16*$^{Ink4a-/-}$ mice. The curves are significantly different ($P <$ 0.0001, log-rank test). We note that no wild-type or *p16*$^{Ink4a-/-}$ mice developed lordokyphosis

during our one-year observation period (data not shown). (**c**) Images of 5-month-old wild-type, *BubR1*$^{H/H}$ and *BubR1*$^{H/H}$;*p16*$^{Ink4a-/-}$ mice. Note the profound difference in the curvature of the spine in the *BubR1*$^{H/H}$;*p16*$^{Ink4a-/-}$ mouse. (**d**) Cross-sections of gastrocnemius muscles from 5-month-old wild-type, *BubR1*$^{H/H}$ and *BubR1*$^{H/H}$;*p16*$^{Ink4a-/-}$ mice. Arrowheads mark degenerated fibres and asterisks mark areas of connective tissue infiltration. Scale bar is 100 μm. (**e**) Quantification of the number of deteriorating (atrophic) muscle fibres in gastrocnemius muscles shown in **d**. Note that *BubR1*$^{H/H}$;*p16*$^{Ink4a-/-}$ muscles have 3-fold less atrophic fibres than *BubR1*$^{H/H}$ muscles. Data are mean ± s.d. (n = 4). (**f**) Skinned 5-month-old wild-type, *BubR1*$^{H/H}$ and *BubR1*$^{H/H}$;*p16*$^{Ink4a-/-}$ mice demonstrating that abdominal wall thickness is visually increased in *BubR1*$^{H/H}$;*p16*$^{Ink4a-/-}$ mice when compared with *BubR1*$^{H/H}$ animals. Scale bar is 1 cm.

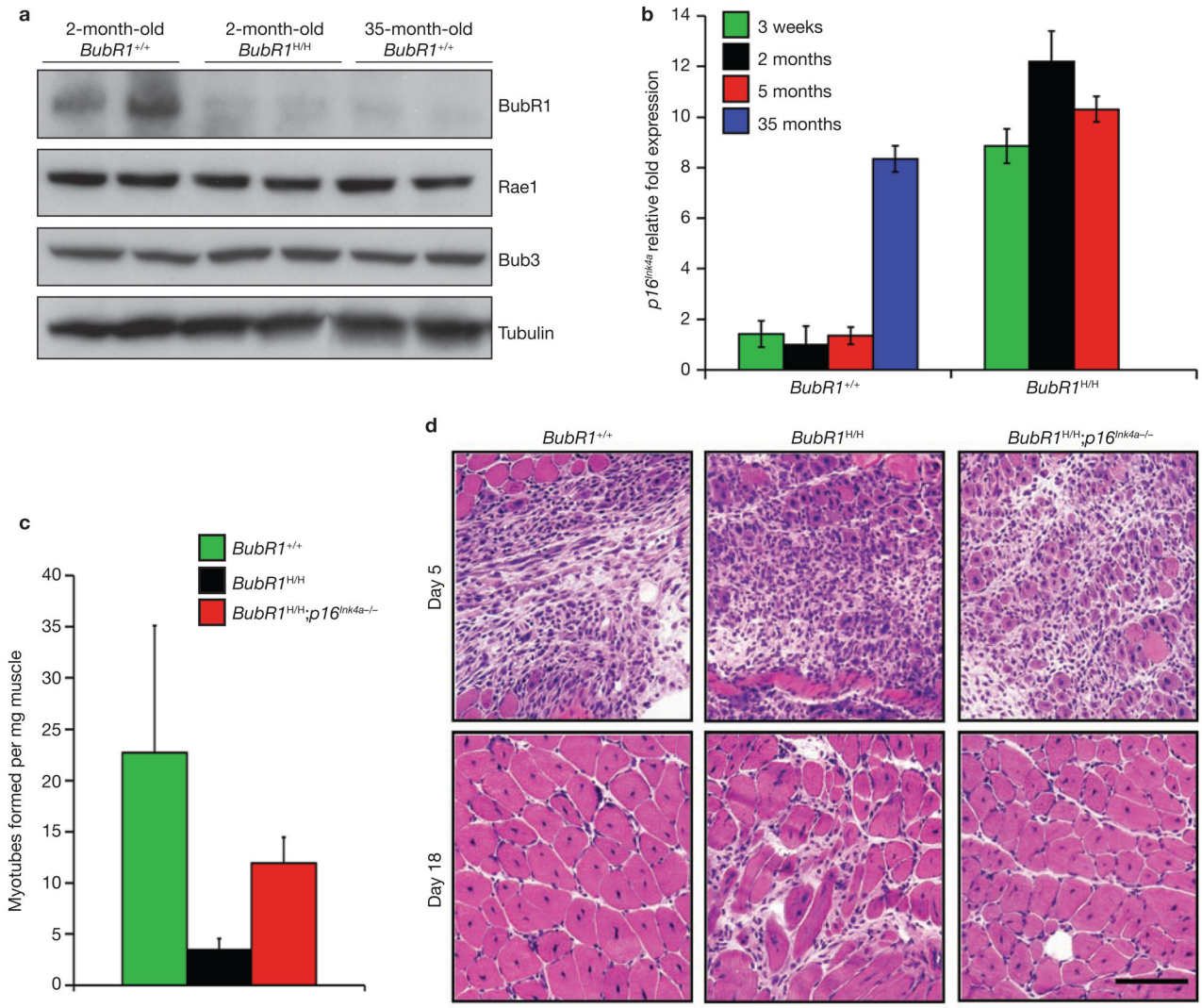

Figure 2.

Inverse correlation between BubR1 and p16^{Ink4a} expression levels with ageing. (**a**) Western blot analysis of gastrocnemius muscle in young wild-type and *BubR1*$^{H/H}$ mice and old wild-type mice. Blots were probed with antibodies against BubR1, Bub3 and Rae1. Anti-tubulin was used as a loading control. Note that the mitotic checkpoint proteins Bub3 and Rae1 remain highly expressed as wild-type mice age. Uncropped images of the scans are shown in Supplementary Information, Fig. S6a. (**b**) *p16*^{Ink4a} expression in wild-type and *BubR1*$^{H/H}$ gastrocnemius muscles at various ages analysed by qRT–PCR. Data are mean ± s.d. (n = 3 males per genotype and age group, with triplicate measurements taken). Values were normalized to *GAPDH*. Relative fold expression is to 2-month-old wild-type values. (**c**) Myotube formation potential of gastrocnemius muscles from 5-month-old mice of the indicated genotypes analysed by a well-standardized *in vitro* assay. Data are mean ± s.d. (n = 4). (**d**) Cardiotoxin-treated gastrocnemius muscle of 5-month-old wild-type, *BubR1*$^{H/H}$ and *BubR1*$^{H/H}$;*p16*$^{Ink4a-/-}$ mice at 5 or 18 days after injection. Note that all gastrocnemius muscles show an extensive hypercellular response to cardiotoxin injection by day 5 regardless of genotype. Wild-type and *BubR1*$^{H/H}$;*p16*$^{Ink4a-/-}$ mice have complete restoration of muscle architecture by myofibres with central nuclei by day 18, whereas *BubR1*$^{H/H}$ mice have been unable to restore normal tissue structure. Scale bar is 100 μm.

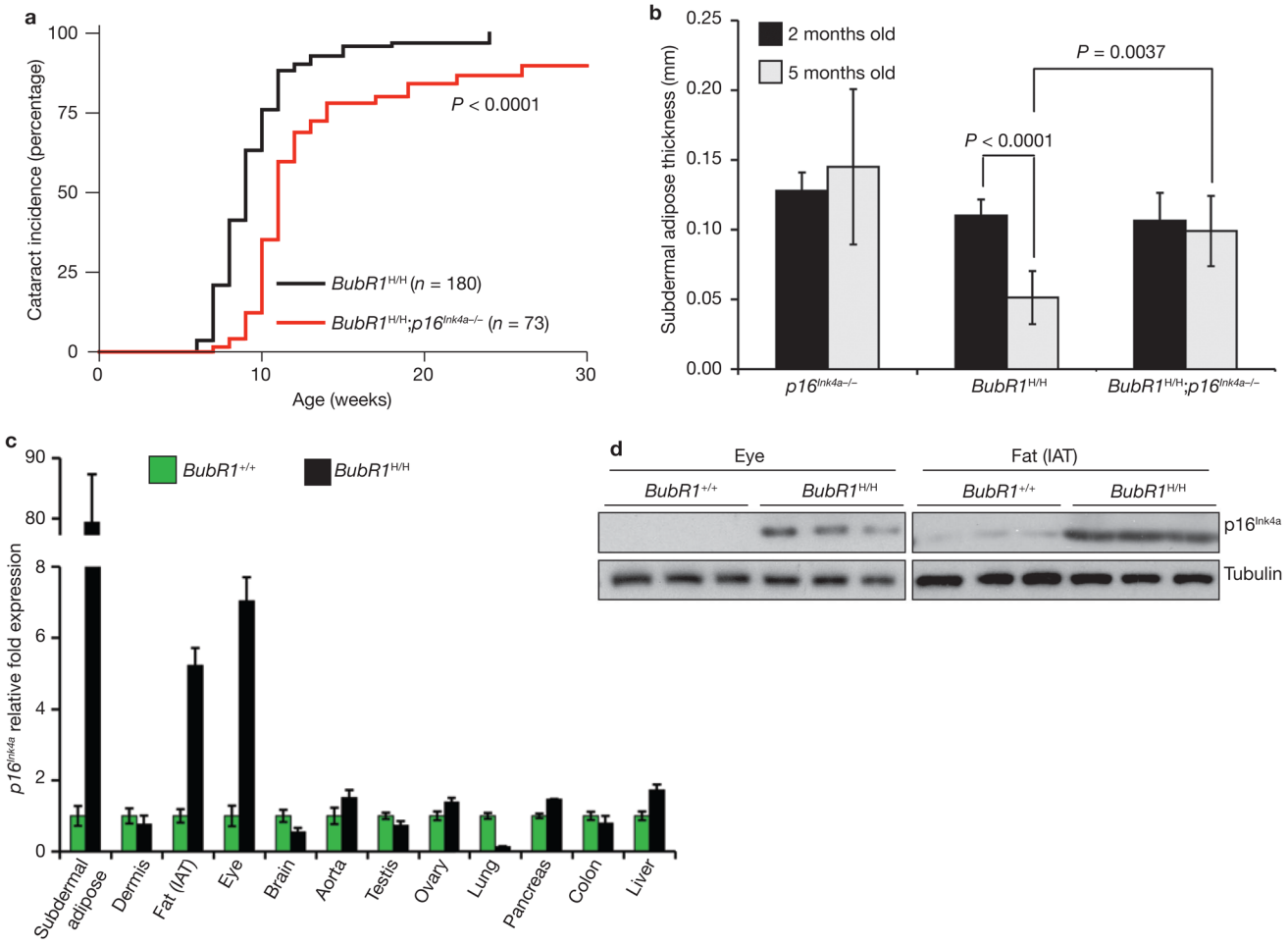

Figure 3. *p16*^{Ink4a} disruption attenuates selective progeroid features of BubR1 hypomorphic mice

(**a**) Incidence and latency of cataract formation in *BubR1*$^{H/H}$ and *BubR1*$^{H/H}$;*p16*$^{Ink4a-/-}$ mice as detected by the use of slit light after dilation of eyes. The curves are significantly different ($P < 0.0001$, log-rank test). We note that no wild-type or *p16*$^{Ink4a-/-}$ mice developed cataracts during this observation period. (**b**) Subcutaneous adipose layer thickness of *p16*$^{Ink4a-/-}$, *BubR1*$^{H/H}$ and *BubR1*$^{H/H}$;*p16*$^{Ink4a-/-}$ mice at 2 and 5 months of age. Data are mean ± s.d. ($n = 4$ male mice for each age per genotype). A two-tailed Mann-Whitney test was used for statistical analysis. (**c**) qRT–PCR analysis for relative expression of *p16*^{Ink4a} in a variety of 2-month-old tissues from *BubR1*$^{H/H}$ and wild-type mice. Values were normalized to *GAPDH*, and relative fold is to 2-month-old wild-type samples. Data are mean ± s.d. ($n = 3$ male mice for each tissue, with triplicate measurements taken). (**d**) Western blots of eye and fat extracts from 2-month-old *BubR1*$^{+/+}$ and *BubR1*$^{H/H}$ mice probed with anti-p16^{Ink4a} antibody. Anti-tubulin antibody served as loading control. Uncropped images of the scans are shown in Supplementary Information, Fig. S6b, c.

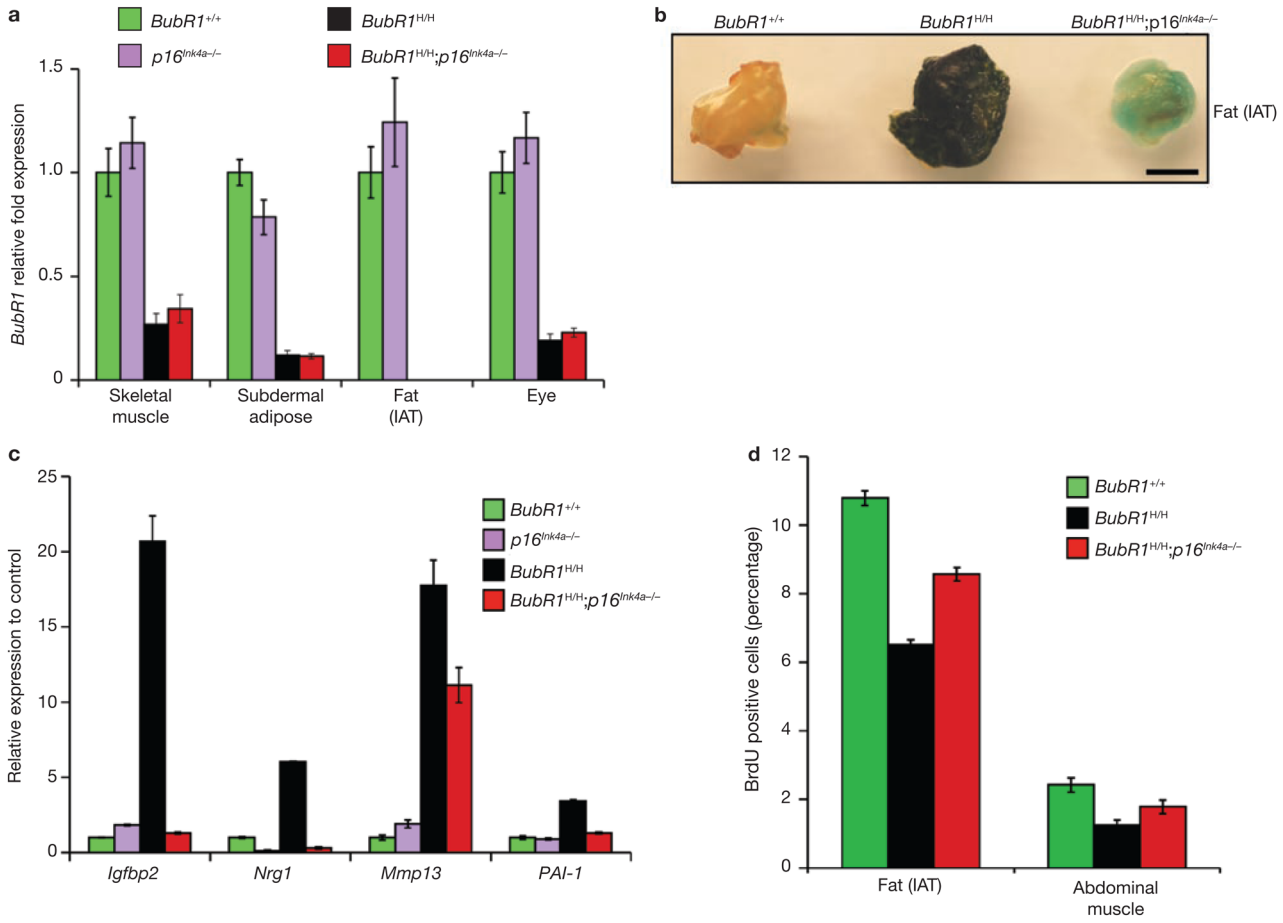

Figure 4. *p16*^{Ink4a} induction in *BubR1*$^{H/H}$ mice promotes cellular senescence

(**a**) Relative expression of BubR1 in gastrocnemius, subdermal adipose, fat deposits and eyes from 2-month-old wild-type, *p16*$^{Ink4a-/-}$, *BubR1*$^{H/H}$ and *BubR1*$^{H/H}$;*p16*$^{Ink4a-/-}$ mice as determined by qRT–PCR. Values were normalized to GAPDH. Relative fold is to 2-month-old wild-type samples. Data are mean ± s.d. (n = 3 male mice per genotype, with triplicate measurements taken per sample). We note that ablation of p16^{Ink4a} was unable to increase the amount of BubR1 present in either wild-type or BubR1 hypomorphic mice. (**b**) IAT of 5-month-old wild-type, *BubR1*$^{H/H}$ and *BubR1*$^{H/H}$;*p16*$^{Ink4a-/-}$ mice stained for SA-β-galactosidase activity. Scale bar is 2 mm. (**c**) Relative expression of senescence markers in gastrocnemius muscles of 2-month-old wild-type, *p16*$^{Ink4a-/-}$, *BubR1*$^{H/H}$ and *BubR1*$^{H/H}$;*p16*$^{Ink4a-/-}$ mice analysed by qRT–PCR. Data are mean ± s.d. (n = 3 male mice per genotype). Values were normalized to *GAPDH*. Relative fold expression is to 2-month-old wild-type muscle. (**d**) Analysis of replicative senescence in skeletal muscle and fat of 2-month-old wild-type, *BubR1*$^{H/H}$ and *BubR1*$^{H/H}$;*p16*$^{Ink4a-/-}$ mice by analysing *in vivo* BrdU incorporation. Data are mean ± s.d. (n = 3 males per genotype).

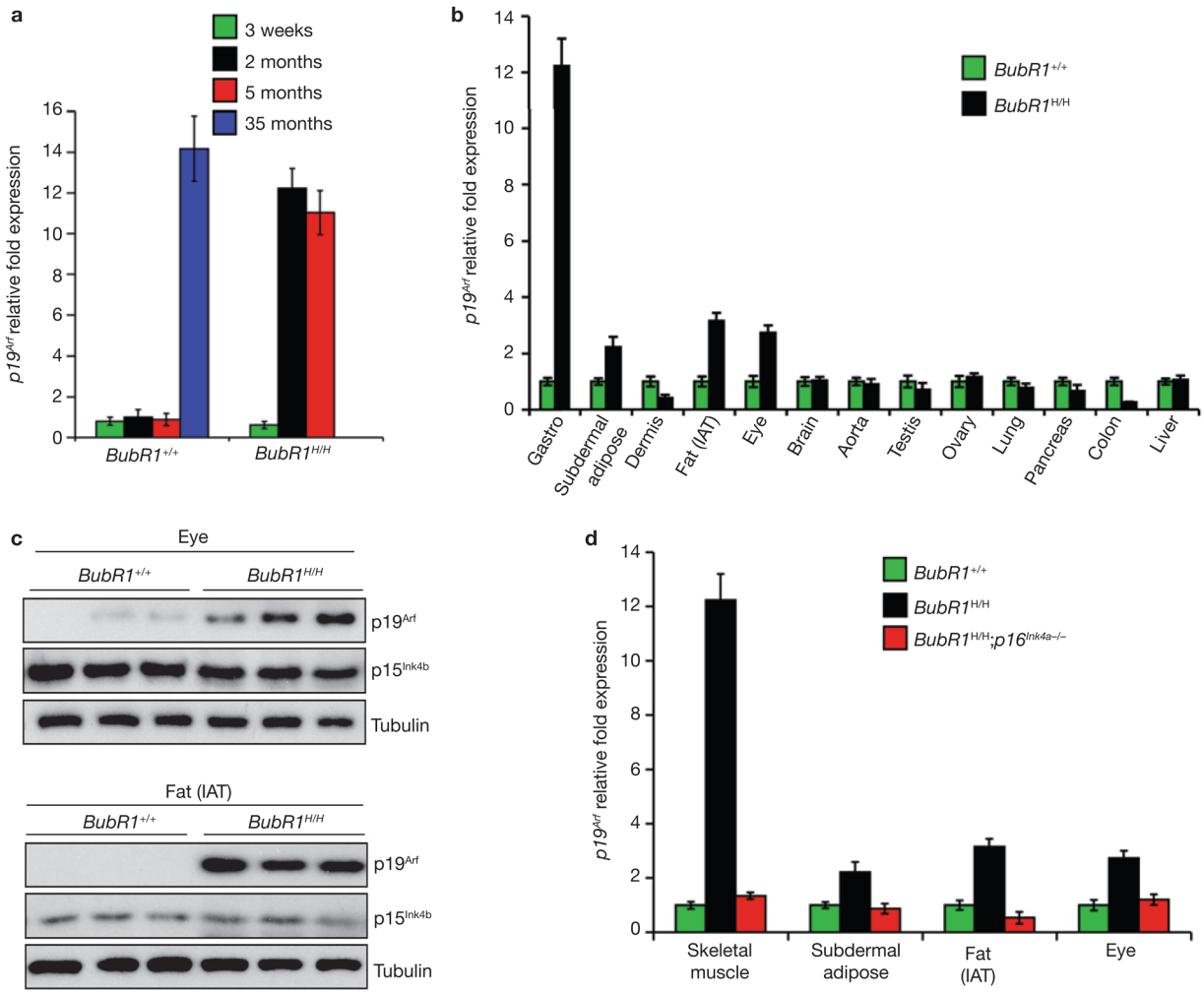

Figure 5.

p19^{Arf} is elevated in BubR1 hypomorphic tissues with high p16^{Ink4a}. (**a**) Skeletal muscles of wild-type and *BubR1*$^{H/H}$ mice of various ages were analysed for *p19*^{Arf} expression by qRT–PCR. All values were normalized to *GAPDH*. Data are mean ± s.d. (*n* = 3 mice were used per genotype and age group). (**b**) Relative expression of *p19*^{Arf} in various tissues of 2-month-old *BubR1*$^{H/H}$ and *BubR1*$^{+/+}$ mice as measured by qRT–PCR. Data are mean ± s.d. (*n* = 3 males per genotype). All values were normalized to *GAPDH*. Relative expression is to wild-type samples. (**c**) Western blots of eye and fat extracts from 2-month-old *BubR1*$^{+/+}$ and *BubR1*$^{H/H}$ mice probed with anti-p19^{Arf} and p15^{Ink4b} antibodies. Anti-tubulin antibody was used as a loading control. Uncropped images of the scans are shown in Supplementary Information, Fig. S6b, c. (**d**) Relative expression of *p19*^{Arf} in skeletal muscle (gastrocnemius), subdermal adipose, fat deposits and eyes of 2-month-old wild-type, *BubR1*$^{H/H}$ and *BubR1*$^{H/H}$;*p16*$^{Ink4a-/-}$ mice as determined by qRT–PCR. Data are mean ± s.d. (*n* = 3 males per genotype). All values were normalized to *GAPDH*. Relative expression is to wild-type samples.

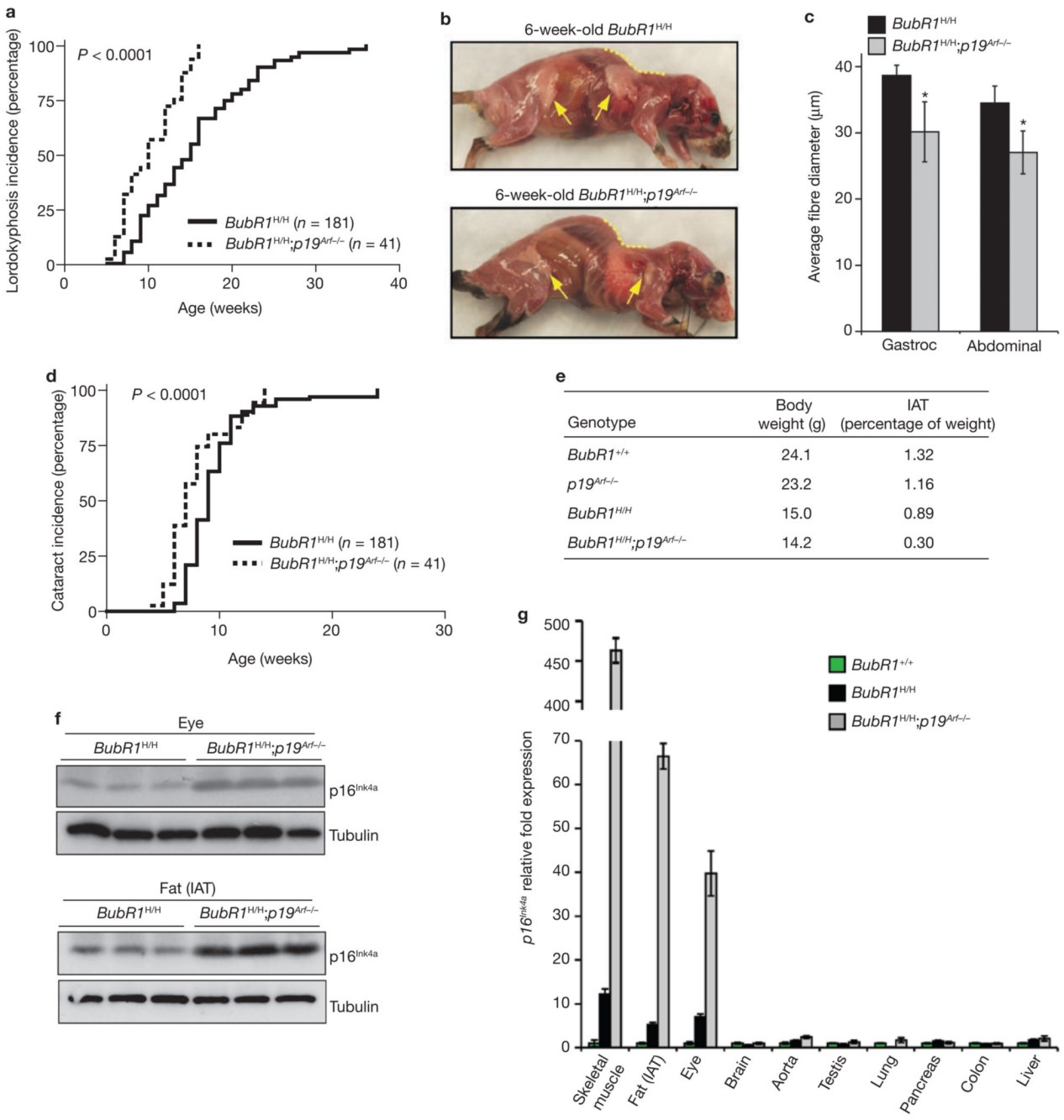

Figure 6.

Accelerated ageing in *BubR1*$^{H/H}$ mouse tissues with increased p16^{Ink4a} expression when p19^{Arf} is lacking. (**a**) Incidence and latency of lordokyphosis in *BubR1*$^{H/H}$ and *BubR1*$^{H/H}$;*p19*$^{Arf-/-}$ mice. The curves are significantly different ($P < 0.0001$, log-rank test). (**b**) Skinned 6-week-old *BubR1*$^{H/H}$ and *BubR1*$^{H/H}$;*p19*$^{Arf-/-}$ males. Note that the *BubR1*$^{H/H}$;*p19*$^{Arf-/-}$ mouse has more profound lordokyphosis (dotted line) and reduced subcutaneous fat deposits (arrows). (**c**) Average muscle fibre size of gastrocnemius (Gastroc) and abdominal muscles of *BubR1*$^{H/H}$ and *BubR1*$^{H/H}$;*p19*$^{Arf-/-}$ males. Data are mean ± s.d. ($n = 3$ mice per genotype). A two-tailed Mann-Whitney test was used for statistics. For both comparisons, $P < 0.0001$. (**d**) Incidence and latency of cataract formation in *BubR1*$^{H/H}$ and

BubR1$^{H/H}$;*p19*$^{Arf-/-}$ mice. The curves are significantly different ($P < 0.0001$, log-rank test). (**e**) Amount of inguinal adipose tissue in 6-week-old mice of the indicated genotypes. IAT is expressed as percentage of total body weight. Three male mice of each genotype were used. (**f**) Western blots of eye and fat extracts from 2-month-old *BubR1*$^{H/H}$ and *BubR1*$^{H/H}$;*p19*$^{Arf-/-}$ mice probed with anti-p16^{Ink4a} and anti-tubulin antibody. Uncropped images of the scans are shown in Supplementary Information, Fig. S6d. (**g**) Relative expression of *p16*^{Ink4a} in various tissues of 2-month-old *BubR1*$^{+/+}$, *BubR1*$^{H/H}$ and *BubR1*$^{H/H}$;*p19*$^{Arf-/-}$ mice as measured by qRT–PCR. Data are mean ± s.d. ($n = 3$ males per genotype). All values were normalized to *GAPDH*. Relative expression is to wild-type samples.

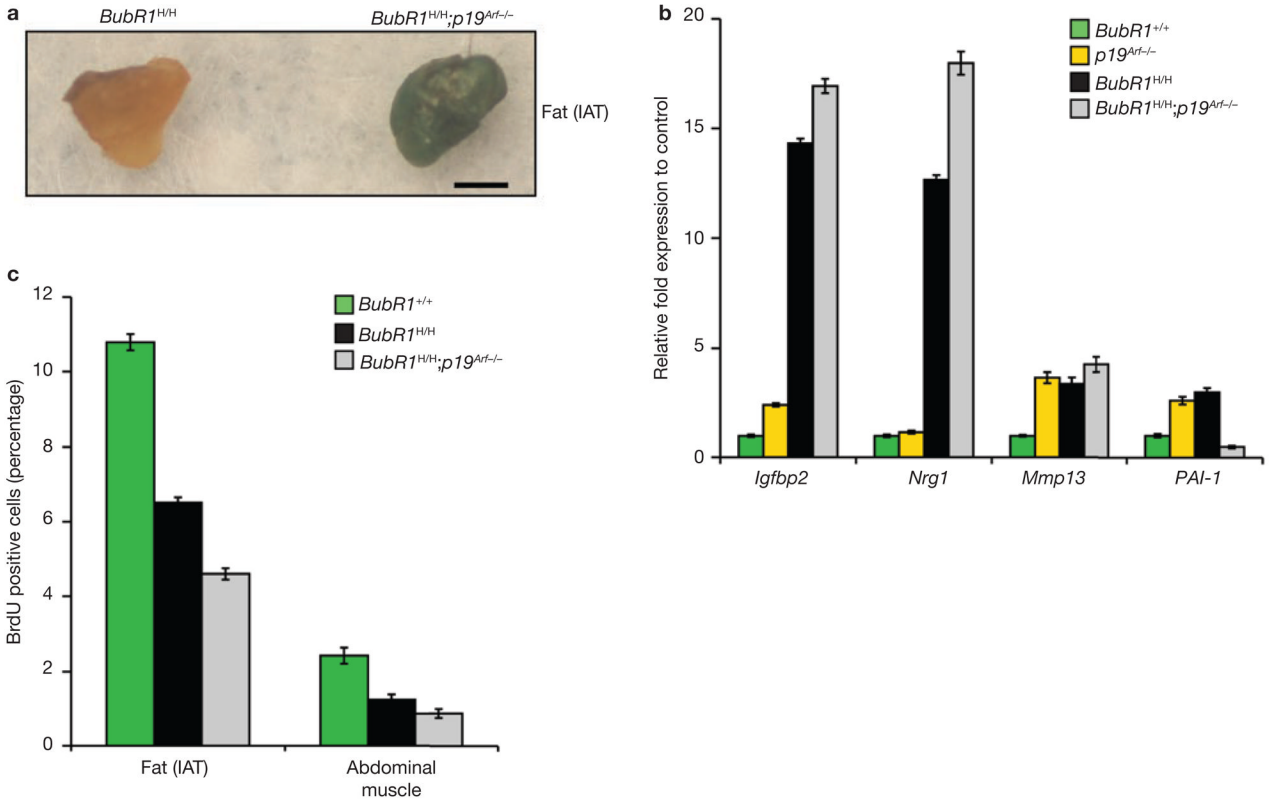

Figure 7.

Senescence increases in *BubR1*$^{H/H}$ tissues with high p16^{Ink4a} when p19^{Arf} is lacking. (**a**) IAT of 2-month-old *BubR1*$^{H/H}$ and *BubR1*$^{H/H}$;*p19*$^{Arf-/-}$ mice stained for SA-β-galactosidase activity. Scale bar is 2 mm. (**b**) Relative expression of senescence markers in gastrocnemius muscles of 6-week-old wild-type, *p19*$^{Arf-/-}$, *BubR1*$^{H/H}$ and *BubR1*$^{H/H}$;*p19*$^{Arf-/-}$ mice. All values were normalized to *GAPDH*. Relative fold expression is to wild-type gastrocnemius. Data are mean ± s.d. ($n = 3$ male mice were evaluated per genotype). (**c**) Replicative senescence in skeletal muscle and fat of 2-month-old wild-type, *BubR1*$^{H/H}$ and *BubR1*$^{H/H}$;*p19*$^{Arf-/-}$ mice as analysed by *in vivo* BrdU incorporation. Data are mean ± s.d. ($n = 3$ male mice per genotype were used for this experiment).

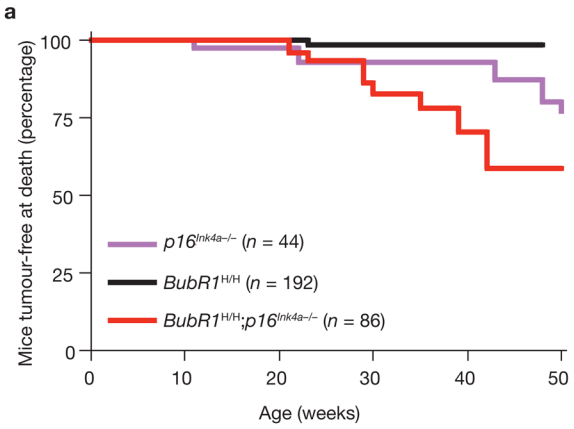

b

Mouse genotype	*BubR1*$^{H/H}$	*BubR1*$^{H/H}$;*p16*$^{Ink4a-/-}$	*p16*$^{Ink4a-/-}$
Tumour type			
Lymphoma	–	–	2%
Lung adenocarcinoma	<1%	9%	–
Hepatocellular carcinoma	–	–	5%
Sarcoma	–	1%	9%

Percentages of tumours from total mice (*n* = 44 *p16*$^{Ink4a-/-}$ mice; *n* = 192 *BubR1*$^{H/H}$; *n* = 86 *BubR1*$^{H/H}$;p16$^{Ink4a-/-}$ mice)

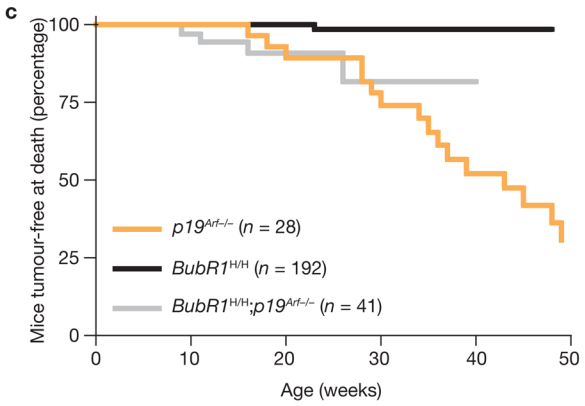

Figure 8.

Ablation of p16^{Ink4a} accelerates lung tumorigenesis in BubR1 insufficient mice. (**a**) Percentage of mice with tumours at time of death as a function of time for *p16*$^{Ink4a-/-}$, *BubR1*$^{H/H}$ and *BubR1*$^{H/H}$;*p16*$^{Ink4a-/-}$ mice. Biopsies were performed on moribund animals and all tissues were screened for tumours. Tumour tissues were collected and processed for histological confirmation. The *BubR1*$^{H/H}$;*p16*$^{Ink4a-/-}$ curve is significantly different from the *BubR1*$^{H/H}$ curve with $P = 0.0027$ (calculated using a log-rank test). (**b**) Tumour spectra of *p16*$^{Ink4a-/-}$, *BubR1*$^{H/H}$ and *BubR1*$^{H/H}$;*p16*$^{Ink4a-/-}$ mice. (**c**) As in **a** but for *p19*$^{Arf-/-}$, *BubR1*$^{H/H}$ and *BubR1*$^{H/H}$;*p19*$^{Arf-/-}$ mice. There is no significant difference between the curves of *BubR1*$^{H/H}$;*p19*$^{Arf-/-}$ and *p19*$^{Arf-/-}$ mice using a log-rank test.